OPEN

Microsystems & Nanoengineering (2015) 1, 15024; doi:10.1038/micronano.2015.24

www.nature.com/micronano

ARTICLE

Biodegradable magnesium/iron batteries with polycaprolactone encapsulation: A microfabricated power source for transient implantable devices

Melissa Tsang[1,*], Andac Armutlulu[2,*], Adam W. Martinez[3], Sue Ann Bidstrup Allen[4] and Mark G. Allen[5]

This study presents the design, fabrication, and testing of biodegradable magnesium/iron batteries featuring polycaprolactone (PCL) as a packaging and functional material. The use of PCL encapsulation minimized the electrochemical cell volume and supported longer discharge lifetimes and higher discharge rates than state-of-the-art biodegradable batteries. Specifically, the electrodes were separated and insulated by a 5 μm-thick PCL layer that served as both a battery packaging material and a permeable coating for physiological solution to penetrate and activate the battery. A systematic investigation of the electrode size, discharge rates, electrolyte selection, and polymeric coating revealed the critical reactions and phenomena governing the performance of the Mg-based biodegradable batteries. Comparison with previous reports on biodegradable batteries and medical-grade non-degradable lithium-ion batteries demonstrated the superior performance of PCL-coated Mg/Fe batteries at these size scales, which exhibited an energy density of 694 Wh kg^{-1} and a total volume of 0.02 cm^3.

Keywords: biodegradable batteries; magnesium electroplating; microfabrication; PCL; transient electronics

Microsystems & Nanoengineering (2015) **1,** 15024; doi:10.1038/micronano.2015.24; Published online: 12 October 2015

INTRODUCTION

Biodegradable electronics have garnered increasing interest as an emerging technology spanning the fields of biomedicine and microelectromechanical systems[1–3]. Specifically, transient implantable medical devices (TIMDs) have been demonstrated, which either entirely or partially dissolve under physiological conditions after completing a sensor task[1,4]. The use of TIMDs would be advantageous in the monitoring and treatment of transient diseases, such as wound healing, bone fracture, traumatic brain injury, and drug delivery systems, in which the devices would only be needed for a transient period. In this respect, TIMDs eliminate the need for revision surgery to remove the devices and the chronic inflammatory response observed with permanently implanted devices. From a cost-benefit perspective, the short period over which a device is required to function for transient disease applications may not warrant the long-term implications associated with permanent implants[5]. Current demonstrations of TIMDs have been limited to either electrically passive designs or wireless powering[5,6]. Hwang *et al.* reported a transient implantable system featuring magnesium (Mg) and silicon nano-membranes[3]. The device was inductively powered and dissolved completely within 10 min. Additional passivation schemes involving magnesium oxide (MgO) and silk were implemented and extended the degradation lifetime to 10 h. Luo *et al.* demonstrated a wireless radio frequency pressure sensor comprising micropatterned zinc (Zn) and iron (Fe) bilayers as the conducting material and poly-L-lactide and polycaprolactone (PCL) as the insulating and structural materials, respectively[1]. The device implemented the galvanic coupling of Zn and Fe to control the conductor degradation rate. Telemetry by inductive coupling, however, is limited to short-range distances (i.e., tens of centimeters)[4] and typically implemented at low frequencies (i.e., less than 100 MHz) with output powers between 10 mW and 250 mW and data rates of 1–2 Mb s^{-1}.

To realize biodegradable devices with higher performance and more advanced functions, appropriately biodegradable energy sources must be developed to provide onboard powering[6]. The development of biodegradable energy sources would support the design of self-powered electronics with greater functionality and permit sensing and actuation over longer time intervals. The global design constraints of a biodegradable energy source are compactness, energy content, performance, shelf life, biodegradability, and biocompatibility. The biodegradable energy source should satisfy the power requirements of the target device utilizing biodegradable chemistries in its operation and degrade into non-toxic products after serving its discharge lifetime. Although transient implantable electronics have not yet reached the commercial market, energy requirements may be estimated based on the power consumption of reported permanent IMDs and the desired functional lifetime of biodegradable analogs. For example, flow rate and pressure sensors may find transient applications in the early detection of vascular graft failure and urodynamic bladder diagnostics. Low-power and ultralow-power (ULP) sensors and telemetry systems have been reported to support implantable medical applications[7–9]. Xue *et al.* reported a blood flow rate sensing system that consumes a total power of 21.6 μW[10]. Majerus *et al.* demonstrated a wireless implantable

[1]School of Biomedical Engineering, Georgia Institute of Technology, Atlanta, GA 30332, USA; [2]School of Chemical and Biomolecular Engineering, Georgia Institute of Technology, Atlanta, GA 30332, USA; [3]School of Electrical and Computer Engineering, Georgia Institute of Technology, Atlanta, GA 30332, USA; [4]Department of Chemical and Biomolecular Engineering, University of Pennsylvania, Philadelphia, PA 19104, USA and [5]Department of Electrical and Systems Engineering, University of Pennsylvania, Philadelphia, PA 19104, USA

*Melissa Tsang and Andac Armutlulu contributed equally to this work.

Correspondence: Mark G. Allen(mallen@seas.upenn.edu)

Received: 30 January 2015; revised: 11 August 2015; accepted: 27 August 2015

micromanometer system that required 32.4 μW of power[11]. In addition, the biodegradable energy source should support current and voltage requirements amenable to microelectronics operation. ULP circuitry is commercially available with current requirements as low as 45 μA MHz^{-1} during active mode and an operating voltage of 0.5[12]. Because biodegradable materials spontaneously break down into their respective principal components in the presence of an aqueous environment (i.e., metals degrade into ionic species and polymers hydrolytically break down into monomers), the design of a biodegradable battery should also emphasize chemistries that support a stable shelf life[13–17]. In addition to minimizing exposure to environmental moisture, this quality also requires minimizing the parasitic corrosion of the electrode materials, defined as dissolution not attributed to energy draw from the battery, in the battery electrolyte, and discharging of the battery prior to intended use[2,6,18].

Because biodegradation may be defined as the electrochemical corrosion of materials within a physiological environment, a natural extension to developing biodegradable electronics is harnessing the energy released from metallic corrosion reactions in the form of a biodegradable battery[19–22]. Tsang *et al.* reported a biodegradable battery comprising micropatterned Mg and Fe as the anode and cathode, respectively, and 0.1 M magnesium chloride as the electrolyte solution[6]. The battery demonstrated a stable discharge potential of 1.1 V at a discharge rate of 125 μA cm^{-2}. However, the electrodes were packaged on bulk silicon, which is not biodegradable, and the study did not demonstrate encapsulation of the proposed electrolyte. Yin *et al.* subsequently demonstrated a series of biodegradable batteries featuring Mg as the anode; Fe, molybdenum (Mo), or tungsten (W) as the cathode; and phosphate-buffered saline (PBS) as the electrolyte[22]. The bulk Mg/Mo cells achieved stable discharge potentials of up to 1.6 V with the use of four cells connected in series at a discharge rate of up to 100 μA cm^{-2}. Kim *et al.* reported an ingestible sodium ion electrochemical cell, composed of manganese oxide (MnO_2) and activated carbon (AC) as the electrode components. The packaged electrochemical cell achieved discharge potentials of up to 0.6 V at discharge currents of 5–20 μA[23]. These demonstrations underscore the prospects of biodegradable batteries for achieving power schemes capable of powering similarly biodegradable devices.

Herein we report a microfabricated PCL-encapsulated Mg/Fe biodegradable battery featuring a total cell volume of less than 0.02 cm^3 and stable performance at discharge rates higher than those previously reported. In addition, this report systematically examines the effect of various design criteria (i.e., electrolyte selection, functional material design, and geometry) on Mg-based batteries and proposes the underlying phenomena governing battery performance. The objective of the present study was twofold: (1) to demonstrate a biodegradable battery with improved discharge performance and (2) to examine Mg-based battery chemistries to support future efforts in developing biodegradable batteries.

MATERIALS AND METHODS

Battery design and operation

Following a functional rather than an electrochemical definition, the devices fabricated in this work will be referred to as PCL-coated Mg/Fe batteries, even though they are more accurately described as electrochemical cells. The PCL-coated Mg/Fe battery featured a two-electrode-cell configuration with Mg as the sacrificial anode and Fe as the cathode. The principle of operation was the galvanic protection of Fe through the anodic oxidation of Mg. As shown in Figure 1a, the electrodes were separated by and encapsulated in a thin PCL film (5 μm thickness) that dually served as the packaging for the battery and a semipermeable membrane for infiltration of the battery electrolyte. The processes by which the battery was microfabricated and assembled are presented in Figure 1b. To overcome challenges associated with electrolyte encapsulation, which requires isolation of the Mg anode from the electrolyte solution prior to the desired activation of the battery, the present study utilized physiological fluid as the battery electrolyte. During testing, PBS was used as an *in vitro* surrogate of physiological fluid.

Magnesium was selected as the anode due to its attractive electrochemical, mechanical, and physiological properties[2,24]. Magnesium exhibits a theoretical-specific capacity of 2200 mAh g^{-1} and a standard electrode potential of 2.34 V *vs*. SHE, which is over 1.5 V more electronegative than Zn and Fe[2,22,25,26]. In addition, Mg features a high modulus-to-density ratio and a Young's modulus (45 GPa) that more closely approximates that of cortical bone (20 GPa) than does titanium or stainless steel (Table 1)[26–28]. Both Mg and Fe have been used in biodegradable structural implants (e.g., bone screws and fixation plates, cardiovascular stents) with confirmed biocompatibility *in vivo*[14,29,30]. Furthermore, Mg^{2+} is the fourth most abundant cation found in

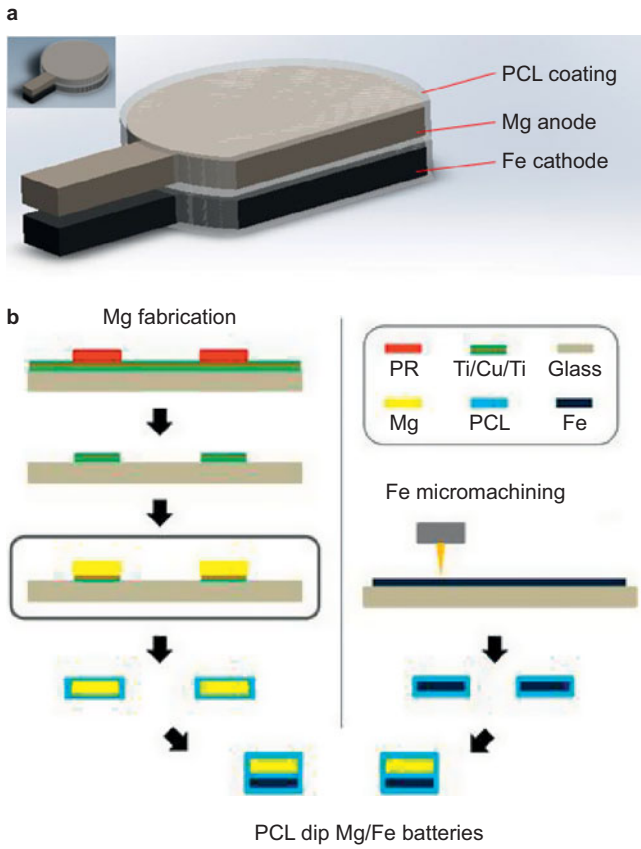

Figure 1 Schematic and fabrication scheme of batteries. (**a**) PCL-coated Mg/Fe batteries that harness physiological solution as the electrolyte. (**b**) The fabrication of PCL dip-coated Mg/Fe batteries comprises three stages: Mg fabrication, Fe micromachining, and battery assembly. Chemical etching through a lithographically defined photomask is performed on a metallized glass substrate to yield a micropatterned seed layer. Magnesium is electrodeposited onto the substrate under a nitrogen atmosphere after removal of the top Ti layer and sample cleaning. Magnesium anodes are then delaminated from the substrate and dip-coated in a PCL solution. Iron cathodes are micromachined from commercial Fe foil with an infrared laser. Samples are removed from the rigid substrate, cleaned, dip-coated into PCL solution, and laminated against the PCL-coated Mg anode to form the assembled battery.

doi:10.1038/micronano.2015.24

Table 1 Comparison of electrochemical, mechanical, and physiological properties of Mg, Zn, and Fe

	Mg	Zn	Fe
Standard electrode potential (V *vs.* SHE)	−2.34	−0.76	−0.44
Theoretical specific capacity (mAh g^{-1})	2200	820	960
Young's modulus (GPa)	45	108	210
Density (g cm^{-3})	1.74	7.14	7.87
Corrosion rate (mil y^{-1})	22.3	1.97	7.48
Daily tolerance (mg)	700	15	15

The electrochemical properties are based on half-cell reactions with a valence of 2.

the body and an essential mineral nutrient[31,32]. Because the anode is consumed in the battery discharge reaction, the high physiological tolerance of Mg supports its use as the sacrificial anode material[33]. In turn, Fe was chosen as the cathode material because it exhibits a more noble electrochemical potential and a lower hydrogen overpotential than that of Zn, providing a more efficient cathode for hydrogen reduction[14,20].

Three electrolytes (0.1 M $MgCl_2$, 0.9 wt.% NaCl, and 1× PBS) were investigated because the ionic constituents of the electrolytes are similarly found in the human body[1,2,6]. Furthermore, the design of a biodegradable battery may either utilize the body's physiological solution as the electrolyte, where PBS is proposed as a suitable analog for *in vitro* studies, or feature encapsulation of the electrolyte cell within biodegradable packaging. Although utilizing physiological solution presents a simpler battery design and facilitates initial battery demonstrations, an investigation of battery performance in alternative electrolytes may support future research on biodegradable batteries with more advanced battery activation and electrolyte isolation mechanisms.

The discharge reactions of the Mg/Fe battery in an aqueous electrolyte are as follows:

$$\begin{aligned}\text{Overall}: &\quad Mg + 2H_2O \rightarrow Mg(OH)_2 + H_2 \quad \Delta E = 1.51\ V\\ \text{Anodic}: &\quad Mg + 2OH^- \rightarrow Mg(OH)_2 + 2e^- \quad E^\circ = -2.34\ V\\ \text{Cathodic}: &\quad 2H_2O + 2e^- \rightarrow H_2 + 2OH^- \quad E^\circ = -0.83\ V\end{aligned}$$

As previously discussed, the oxidation of Mg takes places on the anode surface and reduction of either water or hydrogen occurs on the cathode surface. Hydrogen gas and magnesium hydroxide ($Mg(OH)_2$) are formed from the discharge reactions[2,13,20]. However, additional reactions with electrolyte constituents must also be considered. For example, chloride ions at concentrations greater than 30 mM support the following reactions with Mg:

$$\begin{aligned}Mg + 2Cl^- &\rightarrow MgCl_2 + 2e^-\\ Mg(OH)_2 + 2Cl^- &\rightarrow MgCl_2 + 2OH^-\end{aligned}$$

Both magnesium and magnesium hydroxide react with the reducing chloride environment to form magnesium chloride ($MgCl_2$), a soluble product. The effect is an increased Mg corrosion rate. The following reaction has also been observed with Mg in a phosphate-containing solution:

$$3Mg + 2PO_4^{3-} \rightarrow Mg_3(PO_4)_2 + 6e^-$$

The reaction product, $Mg_3(PO_4)_2$, is less soluble than $MgCl_2$ and occurs as a passivation layer on the Mg surface, with an observable reduction in the corrosion rate and pitting behavior[21]. The cumulative effect of Mg in a multi-ionic species must be considered when understanding the performance of Mg-based battery chemistries.

Fabrication and assembly

Magnesium and iron electrodes were fabricated by non-aqueous electrodeposition and laser micromachining, respectively (Figure 1b). Fabrication of the Mg anodes began with the metallization of glass substrates by DC sputtering (CVC) a 100 nm Ti layer, a 500 nm Cu layer, and a 100 nm Ti layer. A lithographically defined etch mask was deposited onto the substrate using a positive tone photoresist (Shipley S-1813). The photoresist was spun at 3000 rpm at a rate of 500 rpm s^{-1} for 30 s and baked at 110 °C for 3.5 min before ultraviolet exposure and development in tetramethylammonium hydroxide-based aqueous solution (MF-319, Microposit). The exposure dosage was set to 150 mJ cm^{-2} at a wavelength of 365 nm. The Ti and Cu seed layers were chemically etched in dilute hydrofluoric acid (1:50 v/v HF) and ferric chloride ($FeCl_3$) solutions, respectively, to obtain a mesh seed layer featuring the anode geometry and appropriate electrical connections for electroplating. The photoresist and topmost Ti layer were removed by sonication in acetone and with dilute HF, respectively. Electrical connection lines were protected by applying a thin coating of polyvinyl alcohol (1:5 w/v PVA; 2 kDa), which exhibited poor solubility in the electroplating solvent. The samples were dried at room temperature and loaded into a glovebox under dry nitrogen for Mg electroplating. Prior to electroplating, samples were cleaned in a salicylic acid solution (10 g L^{-1} in tetrahydrofuran (THF)) and rinsed in THF[24]. Magnesium electroplating was performed to the desired thickness in a 6:1 molar ratio of methylmagnesium chloride (CH_3MgCl) and aluminum chloride ($AlCl_3$) in THF under pulse plating conditions (i_{av} = 10 mA cm^{-2}, t_{on} = 1 ms, t_{off} = 4 ms, k_{dep} = 7 μm min^{-1})[2]. The electroplated samples were then rinsed in THF and dried.

Iron cathodes were micropatterned from commercial Fe foil (Sigma-Aldrich, St. Louis, Missouri, USA, purity >99.95%) using an infrared laser (Resonetics, Nashua, NH 03060 USA, Nd:YLF, 1047 nm) generating 180 ns pulses at a power density of 18 × 10^{12} W m^{-2}. Prior to laser micromachining, the Fe foil was thoroughly degreased with acetone and laminated onto a glass substrate with adhesive. Following laser micromachining, the samples were immersed in acetone to remove the adhesive, thereby releasing the micromachined Fe cathodes.

Figure 1b shows the assembly and packaging of the microfabricated Mg and Fe electrodes with PCL. The electroplated Mg anodes were delaminated from the glass substrate and dip-coated in a PCL solution (50 mg mL^{-1} in THF). The mass of the Mg anodes was measured by a high-precision balance before and after dip-coating. PCL-coated Mg anodes were stored under an inert nitrogen atmosphere until battery assembly. Iron cathodes were similarly dip-coated in PCL (50 mg mL^{-1} in THF) and laminated with corresponding PCL-coated Mg anodes.

Testing and characterization

Electrochemical testing comprised two phases, beginning with the corrosion assessment of Mg electrodes in various electrolytes. Next, Mg/Fe half-cells were galvanostatically discharged to investigate the effect of electrode size, electrolyte selection, and polymeric passivation. The results were used to produce PCL-coated Mg/Fe full-cell batteries, which were characterized and compared with those reported in previous studies. The corrosion properties of the electroplated Mg anodes in the select electrolytes were investigated by potentiodynamic polarization using a potentiostat (WaveDriver 10, Pine Instruments, Grove City, PA, USA). A three-electrode-cell configuration was implemented with a Mg sample, saturated silver/silver chloride (Ag/AgCl), and a platinum (Pt) mesh as the working, reference, and counter electrodes, respectively. Samples were immersed in the solution for 5 min to reach equilibrium prior to testing. Open-circuit

potentials (OCP) were recorded, and linear sweep voltammetry was conducted for a 1 V range centered at the measured OCP at a scan rate of 1 mV s^{-1}. Corrosion currents were determined from Tafel approximations and polarization resistance in accordance with ASTM G102-89, and the corresponding corrosion rates were determined based on Faraday's law[34]. The electrical conductivity of the electrolyte was measured using a conductivity meter (Bench 700 Series, Oakton Instruments, Vernon Hills, IL, USA), and each sample was measured in triplicate.

The electrochemical performance of the Mg/Fe half-cells and PCL-coated Mg/Fe full-cells was characterized by performing galvanostatic discharge tests in a two-electrode-cell configuration at discharge rates of up to 400 μA cm^{-2} using a potentiostat (Model 263, EG&G Princeton Applied Research, Gaithersburg, Maryland, USA). The electrolyte solutions investigated were 0.1 M $MgCl_2$, 0.9 wt.% NaCl, and 1× PBS, and the electrolyte volume was 50 mL. The cut-off potential for the discharge tests was selected to be 200 mV. Based on the discharge data, the specific capacity (C_s) and the power (P) of the cells were calculated using Equations (1) and (2), where m, I, t, and V_{av} refer to the mass (g), discharge current (mA), discharge time (h), and average discharge potential (V) of the cells, respectively.

$$C_s = \frac{I \cdot t}{m} \quad (1)$$

$$P = V_{av} \cdot I \quad (2)$$

Optical degradation studies were conducted in 1× PBS at 37 °C and agitated at 50 rpm using PCL-coated Mg/Fe full-cells without prior discharge. The medium was exchanged to maintain a pH deviation of less than 0.5 relative to the initial measurements at day 0.

RESULTS

Corrosion behavior of battery electrodes in electrolytes

Magnesium corrodes naturally in aqueous solutions and serves as a sacrificial anode when galvanically coupled with more-noble metals (e.g., Fe and Zn)[6,20]. The consumption of Mg due to natural corrosion (i.e., parasitic corrosion) would reduce the amount of electrochemically active anode material available for battery discharge. Therefore, the assessment of the natural corrosion of the Mg anodes is essential to battery design. As shown in Figure 2, the corrosion potentials of the Mg electrodes were −1.30 V, −1.35 V, and −1.55 V (*vs*. SHE) in 0.1 M $MgCl_2$, 0.9 wt.% NaCl, and 1× PBS, respectively. Fluctuations were observed in the anodic portions of the Mg polarization curves, and they were most pronounced in 0.1 M $MgCl_2$. The corresponding corrosion current, corrosion rate and polarization resistance are summarized in Table 2. Electroplated Mg electrodes demonstrated corrosion current densities of 53.8 μA cm^{-2}, 102 μA cm^{-2} and 24.4 μA cm^{-2} in 0.1 M $MgCl_2$, 0.9 wt.% NaCl, and 1× PBS, which corresponded to corrosion rates of 49 mil yr^{-1}, 93 mil yr^{-1}, and 22 mil yr^{-1}, respectively. The polarization resistance was determined from the linear region within 10 mV of the corrosion potential based on Stern-Gearney equations and corresponded to 1930 Ω cm^{-2}, 666 Ω cm^{-2}, and 1930 Ω cm^{-2} in 0.1 M $MgCl_2$, 0.9 wt.% NaCl and 1× PBS, respectively. The corrosion currents were calculated from the polarization resistance measurements and were in good agreement with Tafel approximations, confirming that the reactions are activation limited. The measured electrolyte conductivity was 0.905 mS cm^{-1}, 7.40 mS cm^{-1}, and 15.9 mS cm^{-1} for 0.1 M $MgCl_2$, 0.9 wt.% NaCl, and 1× PBS, respectively, following the same increasing trend as the corrosion potentials.

Electrochemical performance characterization

Uncoated magnesium half-cells

Figure 3a–d shows the discharge performance of Mg/Fe half-cells in 0.1 M $MgCl_2$. The effect of discharge current density and electrode size was investigated. The Mg electrodes exhibited stable discharge profiles at discharge rates greater than 80 μA cm^{-2} (i.e., 15 μA in Figure 3a). The specific capacity and power of the Mg electrodes showed a parabolic relationship with the discharge rate from 0 μA cm^{-2} to 300 μA cm^{-2} (Figure 3b).

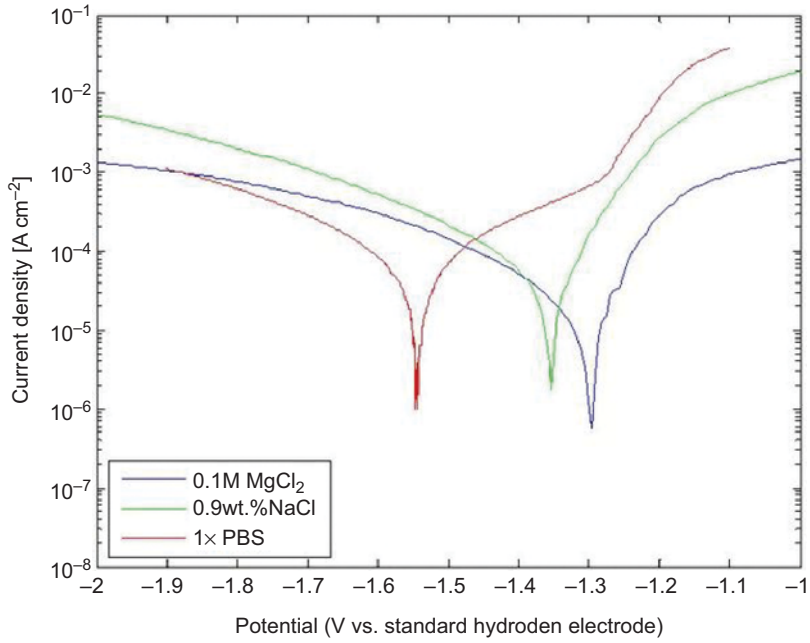

Figure 2 Corrosion behavior of electroplated Mg in physiological solutions. Potentiodynamic sweeps of electroplated Mg in 0.1 M $MgCl_2$, 0.9wt.% NaCl, and 1× PBS showing corresponding corrosion potentials. Tests were performed in 0.1 M $MgCl_2$ using a potentiostat at a sweep rate of 1 mV s^{-1}.

doi:10.1038/micronano.2015.24

Table 2 Comparison of Mg corrosion properties in physiological electrolytes

	0.1 M $MgCl_2$	0.9 wt.% NaCl	1 × PBS
Electrolyte conductivity (mS cm^{-1})	0.905	7.40	15.9
Electrolyte pH	6.09	5.95	7.41
Corrosion potential (V *vs.* SHE)	−1.3	−1.35	−1.55
Corrosion current (μA cm^{-2})	53.8	102	24.4
Corrosion rate (mil yr^{-1})	49.2	93.1	22.3
Polarization resistance (Ω cm^{-2})	1926	666	1932

Conductivity values show the arithmetic mean of three measurements. Corrosion data were obtained from linear sweep voltammetry of electroplated Mg samples against a saturated Ag/AgCl reference electrode and Pt counter electrode.

At the maximum level of performance, which corresponded to 45 μA (230 μA cm^{-2}), the Mg electrodes demonstrated a specific capacity of 770 mAh g^{-1}, an average power of 39 μW, and a Coulombic efficiency of 35%. The Coulombic efficiency of the electrodes was calculated by dividing the mass of the discharged Mg electrode by the mass of the electroplated Mg. Figure 3c–d compares the specific capacity and power of the Mg electrodes for two different anode sizes (i.e., 5 mm and 10 mm diameter). Whereas the parabolic trend was preserved with increasing anode size, the increase in specific capacity with the larger anodes did not scale with the four-fold increase in anode surface area. At 230 μA cm^{-2}, the larger anodes showed a 13% increase in specific capacity. However, increasing the anodic surface area supported higher average powers (Figure 3d), with the maximum power gain observed at 280 μA cm^{-2}, which corresponded to average powers of 36 μW and 108 μW for Mg anodes measuring 5 mm and 10 mm in diameter, respectively.

Improving performance with thin PCL coating

The effect of a protective thin film of PCL was investigated in the half-cell configuration (Figure 3e–h). The PCL dip-coated cells demonstrated smooth discharge profiles but less stable potentials during the tail end of the discharge lifetime. Comparing the discharge profile to that of uncoated electrodes (Figure 3f), the PCL dip-coated half-cells discharged galvanostatically at 55 μA cm^{-2} demonstrated an approximately 400 mAh g^{-1} increase in specific capacity with the additional polymeric coating (5 μm-thick PCL). Figure 3g further shows that the PCL dip-coated Mg electrodes shifted the parabolic trend towards higher discharge rates and higher specific capacities (i.e., to the upper right of the graph) compared to those measured for the uncoated Mg electrodes. As such, the PCL dip-coated Mg electrodes showed lower-specific capacity at 180 μA cm^{-2} than did the uncoated cells but a 70% increase at 280 μA cm^{-2} and a maximum-specific capacity of 930 mAh g^{-1} at 330 μA cm^{-2}. Similarly, the implementation of the PCL coating shifted the parabolic curve towards higher discharge rates (Figure 3h). Specifically, a maximum average power of 41 μW and a Coulombic efficiency of 42% were observed at 330 μA cm^{-2}.

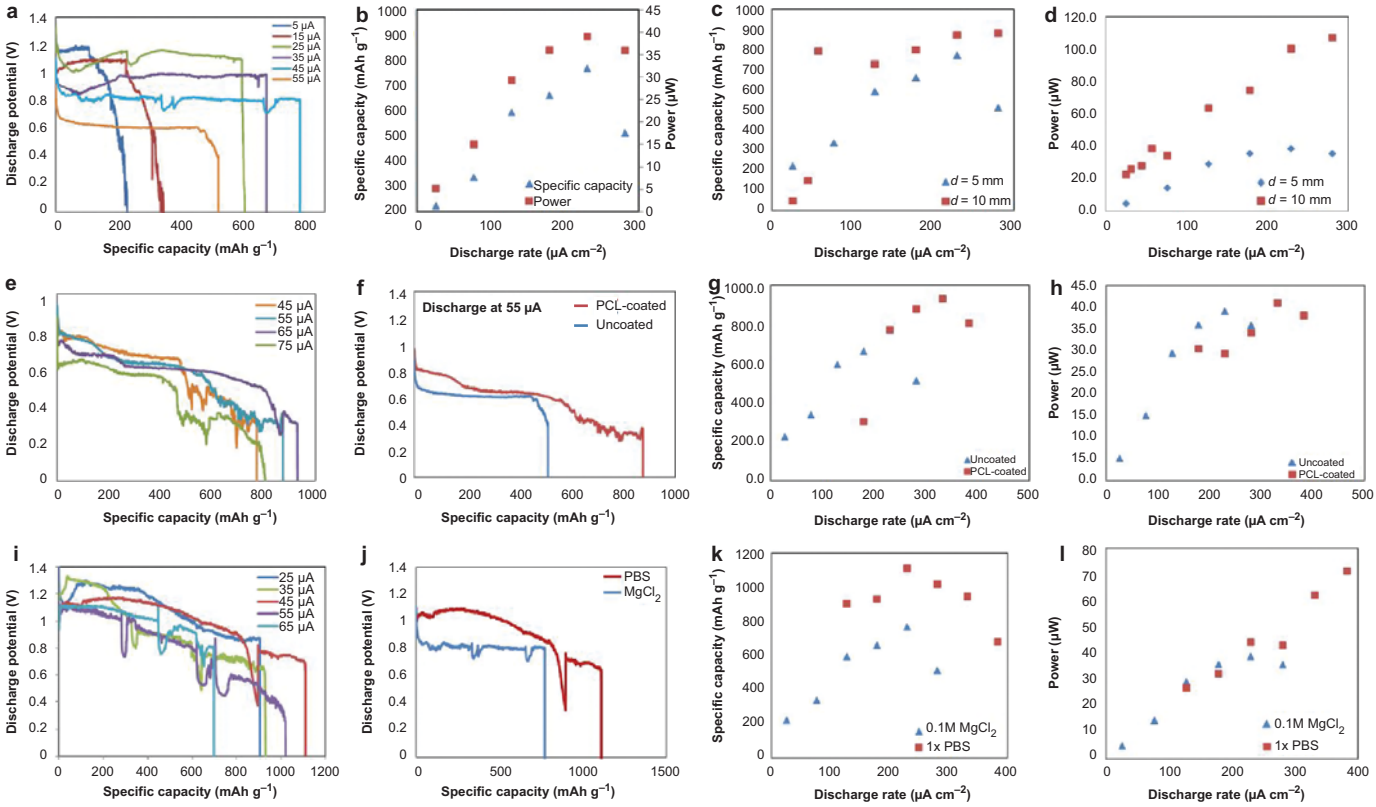

Figure 3 Performance of Mg/Fe half-cells under galvanostatic discharge. (**a**–**d**) Performance in 0.1 M $MgCl_2$; (**e**–**h**) performance with PCL coating; and (**i**–**l**) performance in 1× PBS. (**a**, **e**, and **i**) Discharge profiles of Mg/Fe half-cells at various discharge currents in 0.1 M $MgCl_2$, with PCL coating in 0.1 M $MgCl_2$, and in 1× PBS, respectively; (**b**) Specific capacity and power with discharge rate for 5 mm diameter electrodes. Comparison of (**c**) specific capacity and (**d**) with anode size. (**f**) Effect of PCL at 55 μA. Comparison of PCL-coated and bare electrodes with respect to (**g**) specific capacity and (**h**) power. Comparison of PBS with 0.1 M $MgCl_2$ (**j**) at 45 μA, (**k**) with specific capacity, and (**l**) with power.

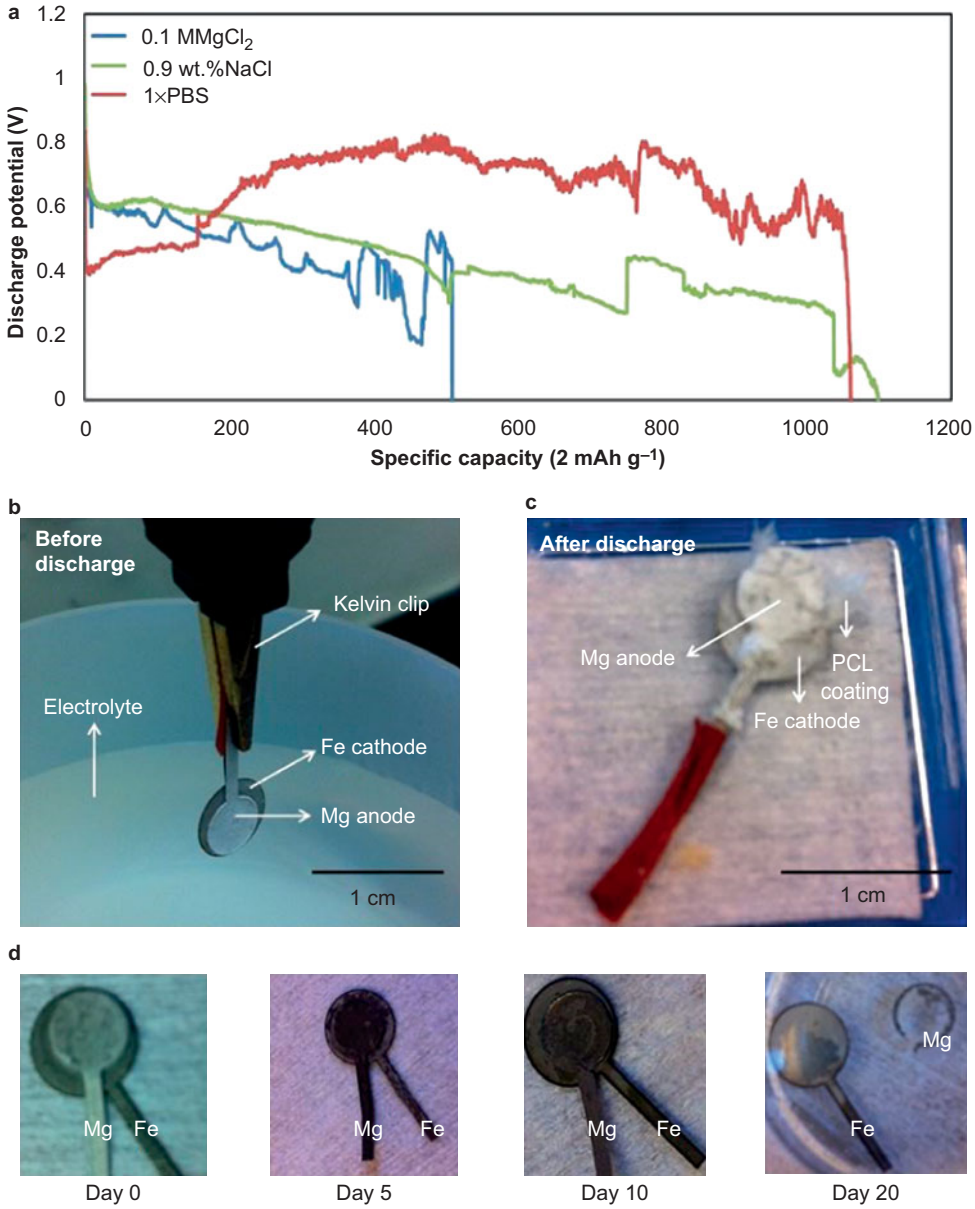

Figure 4 Evaluation of PCL dip-coated Mg/Fe batteries. (**a**) Discharge profiles of PCL dip-coated batteries under galvanostatic discharge at 45 μA in 0.1 M $MgCl_2$, 0.9wt.% NaCl, and 1× PBS. Optical images of assembled PCL dip-coated Mg/Fe battery (**b**) before and (**c**) after discharge at 45 μA. (**d**) Degradation tests were performed in 1× PBS at 37 °C, and samples were not discharged prior to testing to demonstrate the complete dissolution of the biodegradable battery within physiological solution. Nearly, complete dissolution of the Mg anode was observed by day 20. As the degradation rate of Fe occurs on the order of months to years, the time scale of the *in vitro* tests do not capture the Fe degradation process[14,25].

Design trade-offs with electrolyte selection

Figure 3i–l shows the discharge performance of Mg/Fe half-cells in PBS. The discharge potential in 1× PBS was less stable and showed a linear decline throughout the lifetime of the battery compared with the corresponding performance in 0.1 M $MgCl_2$ (Figure 3j). However, the average discharge potential and average power of the Mg electrodes discharged in 1× PBS approximated the values obtained in 0.1 M $MgCl_2$. Figure 3j–k compares the performance of the Mg electrodes in 1× PBS and in 0.1 M $MgCl_2$. Representative profiles of galvanostatic discharge at 45 μA are shown in Figure 3j, indicating that PBS demonstrated a higher average discharge potential and specific capacity than did 0.1 M $MgCl_2$. As shown in Figure 3k, both electrolytes demonstrated a parabolic trend in specific capacity and average power with respect to discharge rate, with the maximum performance centered at 230 μA cm^{-2}. However, for a given discharge rate, uncoated Mg electrodes demonstrated higher-specific capacities in 1× PBS compared to those of electrodes in 0.1 M $MgCl_2$. At 230 μA cm^{-2}, Mg electrodes in 1× PBS exhibited a specific capacity of 1110 mAh g^{-1}, 44% greater than that of the electrodes in 0.1 M $MgCl_2$.

PCL-coated Mg/Fe full-cells

Fully assembled PCL dip-coated Mg/Fe batteries were discharged in 0.1 M $MgCl_2$, 0.9 wt.% NaCl, and 1× PBS (Figure 4a). The batteries were discharged galvanostatically at 45 μA in 50 mL of

doi:10.1038/micronano.2015.24

electrolyte. The discharge profiles were less stable in 0.1 M $MgCl_2$ and 0.9 wt.% NaCl than in 1× PBS. The electrochemical performance of the batteries is summarized in Table 2. The discharge lifetimes were reported to be 49 h, 90 h, and 99 h in 0.1 M $MgCl_2$, 0.9 wt.% NaCl and 1× PBS, respectively. The average discharge potential in 1× PBS was 200 mV and 300 mV greater than in 0.1 M $MgCl_2$ and 0.9 wt.% NaCl, respectively. Furthermore, 0.9 wt.% NaCl and 1× PBS demonstrated similar performance with respect to specific capacity and Coulombic efficiency but more than a two-fold increase compared to 0.1 M $MgCl_2$. The presented PCL dip-coated batteries achieved energies of 3.7 J, 6.2 J, and 11 J in 0.1 M $MgCl_2$, 0.9 wt.% NaCl and 1× PBS, respectively. Optical images of the PCL dip-coated batteries before and after discharge demonstrate the breakdown of the battery due to discharge and natural corrosion (Figure 4c and d). The remainder of the Mg anode after discharge was covered with a white MgO film, and the PCL coating was ruptured.

A separate study of the degradation of the assembled PCL dip-coated Mg/Fe batteries was performed; the results are shown in Figure 4d. The study examined the degradation of the battery assembly in 1× PBS stored at 37 °C and agitated at 50 rpm to mimic body conditions and to assess the lifetime of the implanted battery components. Detachment from the assembly and nearly complete dissolution of the Mg anode was observed by day 20. Because the degradation rate of Fe is well documented in the literature and occurs on the order of months to years, the time scale of the *in vitro* test did not capture the complete cathode degradation process[26].

DISCUSSION

Corrosion behavior of battery electrodes in electrolytes

As shown in Figure 2, Mg exhibited the most noble corrosion potential in 0.1 M $MgCl_2$ and the least noble corrosion potential in 1× PBS. The fluctuations in the anodic curves are indicative of the pitting corrosion characteristic of Mg[2,35]. However, Mg demonstrated the highest corrosion rate in 0.9 wt.% NaCl, which was two-fold and four-fold greater than the corrosion rates observed in 0.1 M $MgCl_2$ and 1× PBS, respectively. This behavior may be attributed to the ionic composition of the electrolytes. It has been reported that the critical chloride concentration required for Mg to undergo pitting corrosion is approximately 30 mM[28]. The chloride concentrations in the physiological electrolytes exceeded the critical concentration and were 200 mM, 154 mM and 140 mM for 0.1 M $MgCl_2$, 0.9 wt.% NaCl and 1× PBS, respectively. Chloride ions react with the $Mg(OH)_2$ passive film on the Mg surface to form a more soluble product, $MgCl_2$. Dissolution of the $Mg(OH)_2$ film reduces the protected surface area and exposes a larger active Mg surface to the electrolyte[18,35]. Although this process suggests that the highest Mg corrosion rate corresponds to the electrolyte with the highest chloride concentration, the interaction of Mg with the remaining electrolyte constituents should also be considered. Although 0.9 wt.% NaCl and 1× PBS exhibited similar concentrations of chloride ions compared to the concentration observed for 0.1 M $MgCl_2$, the Mg corrosion rate in PBS was approximately four-fold lower than that observed in 0.9 wt% NaCl. The presence of phosphate ions may explain the reduced corrosion rate of Mg in 1× PBS. Phosphate ions react with Mg to form a poorly soluble $Mg_3(PO_4)_2$ product that passivates the Mg electrode surface[21]. It should be noted that a lower corrosion rate is not necessarily desirable because the discharge chemistry relies on the continuous formation and breakdown of passivation on the Mg surface. Consequently, the formation of a poorly soluble $Mg_3(PO_4)_2$ film may hinder the anodic reaction on the Mg surface. In contrast, the presence of magnesium ions in 0.1 M $MgCl_2$ may have hindered the dissolution of Mg into the electrolyte solution because a 50% reduction in the corrosion rate was observed with Mg in 0.1 M $MgCl_2$ compared to that observed in 0.9 wt.% NaCl. However, the measured electrical conductivity, which contributes to the total internal resistance of the electrochemical cell, was highest for 1× PBS and lowest for 0.1 M $MgCl_2$, indicating a lower potential drop across the cell when the former electrolyte was utilized. This finding suggests that there exists a design trade-off between solution conductivity and corrosion behavior in electrolyte selection.

Magnesium/iron half-cells

Uncoated half-cells and electrode size

In contrast to conventional battery systems, in which the specific capacity generally increases as the discharge rate is reduced, the Mg electrodes exhibited a parabolic relationship between their discharge rate and specific capacity. The reduced performance at lower discharge rates may be attributed to the pitting nature of Mg. A surface passive film comprising $Mg(OH)_2$ forms when Mg is immersed in an aqueous solution. Pitting corrosion occurs when the $Mg(OH)_2$ film is locally disrupted, exposing the active Mg surface. Because $Mg(OH)_2$ is formed as a reaction product of Mg corrosion, the surface passivation is continually broken down and reformed in pitting zones[18]. When current is drawn from Mg-based batteries, the native passivation is disrupted to initiate battery discharge, as well as corrosion of the anodic material. However, at sufficiently low currents, the rate of $Mg(OH)_2$ reformation is postulated to exceed the rate of film breakdown, resulting in premature termination of the battery. This effect was experimentally observed by discharging a terminated battery, which had previously been discharged at low current (i.e., 5 μA), at elevated current to rupture the reformed passive film and initiate a second interval of discharge (data not shown). In contrast, when high current is drawn from the Mg-based batteries, excessive breakdown of the surface film enhances surface corrosion of the Mg. The parabolic relationship observed between discharge rate and power is attributed to the increased charge transfer resistance and corresponding voltage decline caused by the accumulation and film formation of $Mg(OH)_2$ (Figure 3b). Furthermore, reduced capacity and power have been observed in batteries at high discharge rates due to the limitations pertaining to ion transport as well as kinetics[2,18].

The scalability in performance was investigated with Mg anodes of two sizes. Results indicated that the specific capacity scaled with increasing anodic material, preserving the parabolic trend observed with specific capacity at increasing discharge rates. However, the average discharge power did not scale with increasing anode size because of a voltage drop with larger Mg anodes at higher discharge rates. These findings regarding the scalability of various performance parameters suggest that the surface-area-to-volume ratio may be a critical factor in Mg/Fe battery design.

Improving performance with thin PCL coating

It was hypothesized that a thin protective coating of a biodegradable polymer (e.g., PCL) could enhance the performance of Mg-based batteries by increasing the mechanical integrity of the surface $Mg(OH)_2$ film and, in this manner, enable discharge at higher current densities. This effect was experimentally confirmed with PCL dip-coated electrodes in the half-cell configuration. Although the PCL-coated electrodes supported smooth discharge profiles, the less stable behavior observed during the tail end of the discharge lifetime may have been caused by the steady accumulation of $Mg(OH)_2$ because the polymeric coating may have hindered or slowed down the transport of discharge products from the anode surface. A comparison of the parabolic

trend observed for specific capacity and discharge rate supported the proposed hypothesis (Figure 3g). Implementation of the PCL coating shifted the parabolic trend towards higher discharge rates. This shift reflected the additional charge transfer resistance imposed by the PCL coating, wherein higher current densities were required to break through the PCL-enforced surface passivation. The thin PCL coating improved the specific capacity and Coulombic efficiency of the Mg/Fe electrochemical cells without sacrificing performance with respect to discharge power or potential. Because PCL is an FDA-approved biodegradable polymer, these findings suggest that PCL coatings can be exploited in producing Mg-based biodegradable batteries[4,15,36].

Design trade-offs with electrolyte selection

As discussed previously, the design of a biodegradable battery may comprise two general approaches in terms of electrolyte utilization: (i) placing a specified biocompatible electrolyte within a biodegradable electrolyte cell or (ii) using human physiological fluid as the electrolyte. Although electrochemical testing in 0.1 M $MgCl_2$ supports the former approach, 1× PBS was used to investigate battery performance with physiological solution as the electrolyte. Figure 3j compares the discharge profile in 0.1 M $MgCl_2$ and 1× PBS; as shown, the discharge potential decreased linearly with discharge in PBS. This phenomenon may be attributed to the presence of phosphate ions in PBS, which serves as a pH buffering agent but also reacts with the Mg anode to form an $Mg_3(PO_4)_2$ passivation layer. The passivation presents additional mass transfer resistance at the anode surface. However, the average discharge potential and average power were comparable between 0.1 M $MgCl_2$ and 1× PBS. In fact, Figure 3k indicates that PBS supports higher-specific capacities. Consequently, whereas 0.1 M $MgCl_2$ supports more stable discharge potentials, 1× PBS promoted higher-specific capacities and a longer lifetime for the Mg/Fe half-cells. Figure 3l shows the average powers obtained in 1× PBS and 0.1 M $MgCl_2$, which were comparable at a given discharge rate.

It is speculated that the buffering capacity of PBS promoted the lifetime and specific capacity of Mg-based battery chemistries because Mg is resistant to breakdown in alkaline environments. Studies have reported the accumulation of a thick white film of precipitated $Mg(OH)_2$ when the pH exceeds 9. Magnesium becomes resistant to corrosion when the pH exceeds 10.5 because the elevated pH level corresponds to the pH of saturated $Mg(OH)_2$[20,37]. Given that $Mg(OH)_2$ is a product formed from the oxidation of Mg and its accumulation increases the local pH, the aforementioned effect suggests that the performance of Mg-based batteries may deteriorate or terminate once the electrolyte pH exceeds a critical value indicative of excessive $Mg(OH)_2$ accumulation. Consequently, the buffering system observed in PBS and physiologically in the body may support enhanced battery performance by stabilizing the electrolyte pH as Mg breaks down because of both battery discharge and parasitic corrosion. The buffering capacity of the 1× PBS was experimentally confirmed. It was hypothesized that higher discharge potentials would be attained in 1× PBS due to its higher electrical conductivity. As shown in Table 2, the conductivity of 1× PBS was two orders of magnitude greater than that of 0.1 M $MgCl_2$, thus reducing solution resistance. However, the average power attained in 1× PBS approximated that in 0.1 M $MgCl_2$ because the Mg/Fe half-cells demonstrated similar discharge potentials in the two electrolytes. Furthermore, the average power increased significantly at higher current densities (i.e., >330 μA cm^{-2}) because of the disintegration of the Mg anode at the electrolyte-air interface. This observation served as another indication, as confirmed by corrosion testing (Figure 2), that Mg is more corrosive in PBS.

PCL-coated Mg/Fe full-cells

Figure 4 demonstrates the superior performance of PCL-coated Mg/Fe batteries in PBS, which sustained a higher and more stable discharge potential than batteries discharged in 0.1 M $MgCl_2$ and 0.9 wt.% NaCl. Interestingly, a linear reduction in discharge potential was observed for PCL-coated batteries in 0.1 M $MgCl_2$ and 0.9 wt.% NaCl, which was not observed in corresponding half-cell experiments with uncoated electrodes. In addition, PCL-coated batteries in PBS achieved the longest discharge lifetime and the highest energy, average power and Coulombic efficiency. These results suggest that the application of the PCL coating in the full-cell configuration, which imposes additional mass transfer resistance attributed to the transport of $Mg(OH)_2$, favored PBS as the electrolyte. As mentioned previously, accumulation of the $Mg(OH)_2$ discharge product is mass-transfer- and pH-dependent. Because of the additional mass transfer resistance of the PCL-coated full-cells, the pH buffer system provided by PBS allowed for superior performance as the battery electrolyte. This enhancement was experimentally confirmed by measurements of the electrolyte pH before and after battery discharge (Table 3). As shown, the pH deviated by less than 0.5 throughout the discharge lifetime of the PCL-coated battery in PBS, whereas the changes in the electrolyte pH for batteries discharged in 0.1 M $MgCl_2$ and 0.9 wt.% NaCl were over five- and seven-fold higher, respectively. It is speculated that the buffering capacity of PBS hindered the precipitation of $Mg(OH)_2$, whereas its accumulation during the discharge of the PCL-coated full-cells in 0.1 M $MgCl_2$ and 0.9 wt.% NaCl may have gradually increased charge transfer resistance, accounting for the linear decline in discharge potential.

The discharge performance of the PCL-coated batteries demonstrated promising results for the use of biodegradable batteries to power TIMDs. As discussed previously, the power range required for commercial permanent devices is 10–1000 μW[38]. The power achieved with the PCL-coated batteries satisfies the lower range of IMD power requirements. Specifically, PCL-coated Mg/Fe batteries discharged in PBS achieved an average discharge power and lifetime of approximately 30 μW and 100 h, respectively. This result suggests that the batteries may provide power for low-power neurostimulators for over 4 days[38]. Alternatively, the PCL-coated Mg/Fe batteries may power flow rate sensing systems featuring ULP circuitry for up to 6 days[10].

Comparison to state-of-the-art

The PCL-coated batteries demonstrated improved performance and increased compactness than previously reported biodegradable batteries. Figure 5 compares the energy density and volume of state-of-the-art biodegradable batteries and two commercial lithium-ion (Li-ion) batteries used for medical devices. The fully packaged PCL-coated batteries presented in this study featured a footprint of 0.2 cm^2 and a total volume of less than 0.02 cm^3. These dimensions corresponded to a more than 75-fold reduction in volume compared with that of the Mg/Mo biodegradable

Table 3 Discharge performance of PCL dip-coated Mg/Fe batteries in physiological electrolyte solutions

	0.1 M $MgCl_2$	0.9 wt.% NaCl	1 × PBS
Discharge time (h)	49	90	99
Average discharge potential (V)	0.5	0.4	0.7
Specific capacity (mAh g^{-1})	509	1100	1060
Energy (J)	3.7	6.2	11
Power (μW)	21	19	29
Coulombic efficiency (%)	23	50	48
Change in electrolyte pH	2.11	3.05	0.41

doi:10.1038/micronano.2015.24

battery packaged in polyanhydride (Mg/Mo/PAH) reported by Yin *et al.* in the single-cell configuration (i.e., 3.9 cm^2 and ≈4 mm electrode spacing)[40]. Furthermore, the energy density achieved with PCL-coated Mg/Fe batteries in PBS (694 Wh kg^{-1}) was two orders of magnitude higher than that of the Mg/Mo/PAH battery (four-cell series connection)[39]. The reported battery also featured a smaller volume and higher energy density compared to the edible sodium-ion electrochemical cells reported by Kim *et al.*, which featured AC and manganese dioxide electrodes (AC/MnO_2) on a conductive polymer film (i.e., silver nanowires dispersed in polyglycerol sebacate)[23]. Although Kim *et al.* subsequently presented a melanin-based (Mel/MnO_2) sodium ion cell, which demonstrated improved performance with an energy density of 16.6 Wh kg^{-1}, results did not feature full-cell design and packaging[40]. Comparing with commercial primary Li-ion batteries, the reported PCL-coated Mg/Fe batteries exhibited greater compactness by harnessing physiological solution as the electrolyte and a low-density element as the sacrificial anode material. The PCL-coated battery also featured a higher energy density than the densities exhibited by lithium-manganese dioxide (Li-MDX) and lithium-carbon monofluoride (Li-CFx) batteries, i.e., demonstrated 149 Wh kg^{-1} and 200 Wh kg^{-1}, respectively[41,42].

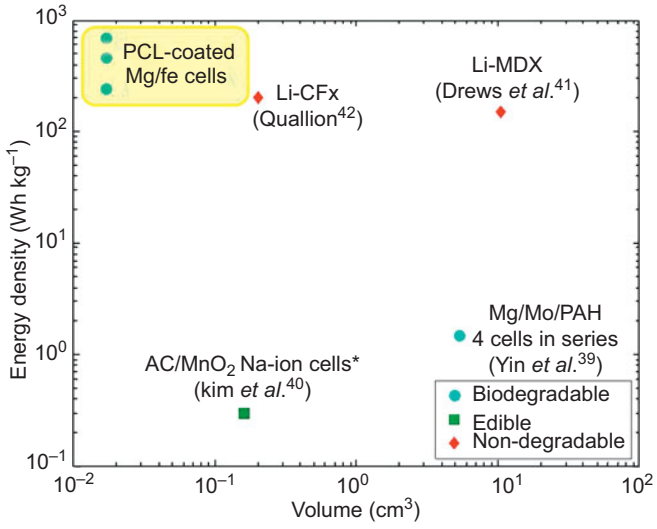

Figure 5 Energy density *vs*. volume of reported biodegradable and edible energy sources. To evaluate the design constraints of battery performance and compactness, energy density, and volume of biodegradable, and edible energy sources are compared with commercial primary batteries (i.e., Li-CFx and Li-MDX). (*denotes data for batteries without packaging).

In addition, the reported PCL-coated Mg/Fe batteries maintained stable discharge performance at higher discharge rates and longer discharge times than previously reported biodegradable batteries. Yin *et al.* implemented a series of four cells to obtain an average potential of 1.6 V for a discharge lifetime of 6 h[39]. In this study, the PCL-coated batteries achieved an average potential of 0.7 V in the single-cell configuration, and the microfabrication process (Figure 1b) supports batch-scale production and modifications for series configuration. The PCL-coated batteries further demonstrated a more than 16-fold improvement in battery lifetime. Through the implementation of a thin PCL coating that could serve as a packaging material and provide passivation enhancement, the reported PCL-coated Mg/Fe cells supported higher discharge rates than those reported for alternative galvanic-based biodegradable batteries. Yin *et al.* observed a limiting current density of 100 μA cm^{-2} in the Mg/Mo/PAH galvanic cell, above which the discharge potential significantly deteriorated. Consequently, the multicell Mg/Mo battery featured an electrode area of 10.5 cm^2 to attain an output current of 700 μA[39], corresponding to a current density of 66.7 μA cm^{-2}. In the present study, stable battery discharge was achieved at current densities of up to 400 μA cm^{-2}. This performance facilitated miniaturization of the biodegradable battery compared to previous demonstrations while improving performance. The PCL-coated batteries achieved a Coulombic efficiency of 50% and an energy efficiency of 22.5%. More broadly, the trajectory of improvement demonstrated by these results suggests that biodegradable batteries present a viable strategy for achieving self-powered TIMDs at clinically relevant time scales and in device power schemes.

CONCLUSION

This study investigated the effects of electrolyte selection, geometry, and a thin PCL coating on the performance of biodegradable Mg/Fe batteries. Results indicated that the use of physiological fluid as the electrolyte, where PBS served as an *in vitro* surrogate, may enhance battery performance over that provided by alternative electrolytes because of its pH-buffering abilities. It was further observed that the surface passivation of $Mg(OH)_2$ on the Mg anode largely governs battery performance, where enhancing the mechanical integrity of passivation with a thin polymeric coating supported higher discharge rates and specific capacities. Thus, this study demonstrated the microfabrication and testing of PCL-coated Mg/Fe biodegradable batteries. Using physiological fluid as the electrolyte and thin PCL coatings for packaging and improved discharge performance, the presented batteries demonstrated longer lifetimes and higher discharge rates than those reported in previous studies on biodegradable batteries. The PCL-coated batteries sustained an average power of approximately 30 μW for 100 h, which is sufficient for powering a commercial pacemaker for up to 4 days. Furthermore, the battery design satisfies the design constraint of compactness, occupying a volume of less than 0.02 cm^3. The promising discharge performance and verified biodegradation of the PCL-coated Mg/Fe batteries support the consideration of the batteries as potential energy sources for powering transient implantable medical devices.

ACKNOWLEDGEMENTS

The authors would like to thank Richard Shafer for his technical assistance. The authors also greatly acknowledge the valuable comments and suggestions of Dr. Thomas F. Fuller.

COMPETING INTERESTS

The authors declare no conflict of interest.

REFERENCES

1 Luo M, Adam WM, Chao S *et al.* A microfabricated wireless RF pressure sensor made completely of biodegradable materials. *Journal of Microelectromechanical Systems* 2014; **23**: 4–13.
2 Tsang M, Andac A, Florian H *et al.* Development of electroplated magnesium microstructures for biodegradable devices and energy sources. *Journal of Microelectromechanical Systems* 2014; **23**: 1281–1289.
3 Hwang S-W, Hu T, Dae-Hyeong K *et al.* A physically transient form of silicon electronics. *Science* 2012; **337**: 1640–1644.
4 Boutry CM, Hengky C, Patrick S *et al.* Towards biodegradable wireless implants. *Philosophical Transactions of the Royal Society of London A: Mathematical, Physical and Engineering Sciences* 2012; **370**: 2418–2432.
5 Allen MG. Microfabricated implantable wireless microsystems: Permanent and biodegradable implementations. IEEE 27th International Conference on Micro Electro Mechanical Systems (MEMS); 26–30 Jan 2014; San Francisco, CA, USA; 2014: 1–4.

6 Tsang M, Andac A, Adam M *et al.* A MEMS-enabled biodegradable battery for powering transient implantable devices. IEEE 27th International Conference on Micro Electro Mechanical Systems (MEMS), 26–30 Jan 2014; San Francisco, CA, USA; 2014: 358–361.
7 Kilian G, Hristo P, Psiuk R *et al.* Improved coverage for low-power telemetry systems using telegram splitting. Proceedings of 2013 European Conference on Smart Objects, Systems and Technologies (SmartSysTech), 11–12 Jun 2013; Erlangen, Germany; 2013: 1–6.
8 Turcza P. An ultra low power 2 Mbps RF-telemetry system for neural recording applications. *Procedia Engineering* 2012; **47**: 813–816.
9 Garcia-Alonso S, Bautista T, Sosa J *et al.* Low-power MEMS pressure sensor for wireless biomedical applications. IEEE 54th International Midwest Symposium on Circuits and Systems (MWSCAS); 7–9 Aug 2011; Seoul, South Korea; 2011: 1–4.
10 Xue R-F, Jia HC, Hyouk-Kyu C *et al.* Ultra-low-power wireless implantable blood flow sensing microsystem for vascular graft applications. 13th International Symposium on Integrated Circuits (ISIC); 12–14 Dec 2011; Singapore, Singapore; 2011: 224–229.
11 Majerus SJA, Steven LG, Michael AS *et al.* Wireless, ultra-low-power implantable sensor for chronic bladder pressure monitoring. *ACM Journal on Emerging Technologies in Computing Systems (JETC)* 2012; **8**: 11.
12 Texas Instruments. *MSP430 Ultra-Low-Power Microcontrollers*, 2014. Available at http://www.ti.com/lit/sg/slab034ab/slab034ab.pdf.
13 Yun Y, Zhongyun D, Namheon L *et al.* Revolutionizing biodegradable metals. *Materials Today* 2009; **12**: 22–32.
14 Moravej M, Diego M. Biodegradable metals for cardiovascular stent application: Interests and new opportunities. *International Journal of Molecular Sciences* 2011; **12**: 4250–4270.
15 Razak SIA, Sharif N, Rahman WAWA. Biodegradable polymers and their bone applications: A review. *International Journal of Basic & Applied Sciences* 2011; **12**: 31–49.
16 Gentile P, Valeria C, Irene C *et al.* An overview of poly (lactic-co-glycolic) acid (PLGA)-based biomaterials for bone tissue engineering. *International Journal of Molecular Sciences* 2014; **15**: 3640–3659.
17 She Didi, Melissa T, Jungkwun K *et al.* Immobilized electrolyte biodegradable batteries for implantable MEMS. The 18th International Conference on Solid-State Sensors, Actuators and Microsystems (TRANSDUCERS); 21–25 Jun 2015; Anchorage, AK, USA; 2015: 494–497.
18 Thomas B, Linden D, Thomas R. *Linden's Handbook of Batteries*. McGraw-Hill Education, New York, USA, 2010.
19 Gill P, Norman M, Rupak D *et al.* Corrosion and biocompatibility assessment of magnesium alloys. *Journal of Biomaterials and Nanobiotechnology* 2012; **3**: 10–13.
20 Song GL, Andrej A. Corrosion mechanisms of magnesium alloys. *Advanced Engineering Materials* 1999; **1**: 11–33.
21 Xin Y, Chenglong L, Xinmeng Z *et al.* Corrosion behavior of biomedical AZ91 magnesium alloy in simulated body fluids. *Journal of Materials Research* 2007; **22**: 2004–2011.
22 Vojtěch D, Kubásek J, Šerák J *et al.* Mechanical and corrosion properties of newly developed biodegradable Zn-based alloys for bone fixation. *Acta Biomaterialia* 2011; **7**: 3515–3522.
23 Kim YJ, Sang-Eun C, Jay W *et al.* Self-deployable current sources fabricated from edible materials. *Journal of Materials Chemistry B* 2013; **1**: 3781–3788.
24 Tsang M, Florian H, Richard HS *et al.* Methods for the microfabrication of magnesium. IEEE 26th International Conference on Micro Electro Mechanical Systems (MEMS); 20–24 Jan 2013; Taipei; 2013: 347–350.
25 Aurbach D, Alexander S, Moty M *et al.* On the mechanisms of reversible magnesium deposition processes. *Journal of the Electrochemical Society* 2001; **148**: A1004–A1014.
26 Hermawan H, Maryam M, Dominique D *et al.* Degradation behaviour of metallic biomaterials for degradable stents. *Advanced Materials Research* 2007; **15**: 113–118.
27 Correia V, Vitor S, Martins MS *et al.* Piezoresistive sensors for force mapping of hip-prostheses. *Sensors and Actuators A: Physical* 2013; **195**: 133–138.
28 Witte F, Norbert H, Carla V *et al.* Degradable biomaterials based on magnesium corrosion. *Current Opinion in Solid State and Materials Science* 2008; **12**: 63–72.
29 Witte F. The history of biodegradable magnesium implants: A review. *Acta Biomaterialia* 2010; **6**: 1680–1692.
30 Xue D, Yeoheung Y, Zongqing T *et al. In vivo* and *in vitro* degradation behavior of magnesium alloys as biomaterials. *Journal of Materials Science & Technology* 2012; **28**: 261–267.
31 Fawcett WJ, Haxby EJ, Male DA. Magnesium: Physiology and pharmacology. *British Journal of Anaesthesia* 1999; **83**: 302–320.
32 Saris Nils-Erik L, Eero M, Heikki K *et al.* Magnesium: An update on physiological, clinical and analytical aspects. *Clinica Chimica Acta* 2000; **294**: 1–26.
33 Gu X-N, Yu-Feng Z. A review on magnesium alloys as biodegradable materials. *Frontiers of Materials Science in China* 2010; **4**: 111–115.
34 ASTM G102-89. Standard practice for calculation of corrosion rates and related information from electrochemical measurements, 2010.
35 Walter R, Bobby KM. Influence of surface roughness on the corrosion behaviour of magnesium alloy. *Materials & Design* 2011; **32**: 2350–2354.
36 Williams JM, Adebisi A, Rachel MS *et al.* Bone tissue engineering using polycaprolactone scaffolds fabricated via selective laser sintering. *Biomaterials* 2005; **26**: 4817–4827.
37 Pourbaix M. Electrochemical corrosion of metallic biomaterials. *Biomaterials* 1984; **5**: 122–134.
38 Wei X, Jing L. Power sources and electrical recharging strategies for implantable medical devices. *Frontiers of Energy and Power Engineering in China* 2008; **2**: 1–13.
39 Yin L, Xian H, Hangxun X *et al.* Materials, designs, and operational characteristics for fully biodegradable primary batteries. *Advanced Materials* 2014; **26**: 3879–3884.
40 Kim YJ, Wei W, Sang-Eun C *et al.* Biologically derived melanin electrodes in aqueous sodium-ion energy storage devices. *Proceedings of the National Academy of Sciences* 2013; **110**: 20912–20917.
41 Drews J, Fehrmann G, Staub R *et al.* Primary batteries for implantable pacemakers and defibrillators. *Journal of Power Sources* 2001; **97**: 747–749.
42 Quallion LLC. Non-rechargeable Lithium-ion Battery: QL0025C, 2003.